A method for determination of frequency-dependent effective scatterer number density

Jian-Feng Chen
Department of Medical Physics, University of Wisconsin, Madison, Wisconsin 53706

Ernest L. Madsen
Department of Medical Physics, University of Wisconsin, Madison, Wisconsin 53706

James A. Zagzebski
Department of Medical Physics, Radiology, and Human Oncology, University of Wisconsin, Madison, Wisconsin 53706

(Received 15 February 1993; revised 20 May 1993; accepted 20 September 1993)

Previous researchers have shown that for low scatterer concentrations, the scatterer number density in an ultrasound pulse-echo experiment can be obtained from ratios of the fourth to the second moment of the backscattered signal. In this paper a new method is presented for determining an *effective scatterer number density*, which is the actual number density multiplied by a frequency-dependent factor that depends on the differential scattering cross sections of all scatterers. The method of data reduction goes beyond the work of previous authors in that, in addition to accounting for the possibility that different sets of scatterers may dominate the echo signal at different frequencies, it also explicitly retains both the temporal nature of the data acquisition and the properties of the ultrasound field in the data reduction. Tests of the method in phantoms yielded good agreement between measured values of the effective scatterer number density and number densities calculated using first principles.

PACS numbers: 43.20.Gp, 43.20.Jr, 43.20.Fn, 43.35.Cg

INTRODUCTION

Ultrasonic backscattering from tissue has the character of random signals. This is caused by random inhomogeneities of the acoustic properties of biological tissues and is responsible for the "speckle" pattern observed on clinical *B*-mode images. These random signals contain useful information related to the scattering structures of tissue. For example, the backscatter coefficient is obtained from the second moment of the backscatter signal.[1] In this paper we will describe a method for extracting a new tissue characterization parameter called the effective scatterer number density from the second and fourth moments of backscattered signals.

The backscattered signal results from a superposition of waves scattered from weak, randomly distributed inhomogeneities in tissue. When the number of randomly positioned inhomogeneities (scatterers) is large enough, applying the central limit theorem, the statistical properties of these signals approach those of a Gaussian distribution. Thus, the real and imaginary parts of the scattered signal are zero-mean, jointly Gaussian random variables, and the magnitude of the backscattered signal follows a Rayleigh distribution.[2] However, if the number of scatterers in a "resolution cell," defined by the ultrasound beam profile and the emitted pulse shape, is small enough[3] and/or if there are clustered scattering structures involved,[4] the backscattered signals will deviate from a Gaussian distribution. Such conditions may be common, for example, in high-resolution ultrasound imaging or when a low scatterer concentration is present.

Kuc[5] used a parameter called the kurtosis to characterize scattering from tissue based on the deviation of the backscattered signal amplitude distribution from that of a Rayleigh distribution. Sleefe[6,7] developed this concept further to estimate the scatterer number density. The scatterer number density has shown promise for differentiating normal from abnormal tissue.[8] Weng[4] proposed a model previously applied in optics[9] to analyze speckle statistics under conditions of low scatterer concentration. This model could also be applied to estimate the scatterer number density.

Most of these models do not set up a clear relationship between the scatterer number density and other properties of the scattering medium. For example, the effect of frequency on the result has not been considered, even though this may be important for biological tissue. In the case of human liver, for example, it has been proposed that there are two sets of scatterers, one set being on the order of a millimeter in size, and the other set being in the range of 20–40 μm.[10] Each set would dominate the backscatter signal at different frequency ranges.

Other difficulties with previous models for estimating scatterer number density include use of approximations to obtain the scattering volume. Sleefe and Weng have taken the volume of scatterers involved to be bounded laterally by the -3-dB beamwidth in the gated region. Another approximation is that, corresponding to a segment of an echo signal, there exist two planar surfaces perpendicular to the axis of the transducer that bound the scatterers contributing to the signal. Two such bounding surfaces will exist, but they are not planar; each surface likely has a shape lying between a plane and a spherical surface, the

 0001-4966/94/95(1)/77/9/$6.00

latter having its center at the center of the transducer surface.[1]

In this article, we describe a method to determine a parameter termed the "effective scatterer number density" which avoids the uncertainties described above. The parameter is clearly defined and can be accurately determined without making the above approximations.

I. THEORETICAL MODEL

A. A review of the backscatter signal from a random medium

Symbols used in this article are largely those used by Madsen *et al.*[1] We consider the situation where a pulsed transducer is used to insonify a medium containing scatterers. Several assumptions are made prior to the analysis of backscattered signals from this medium. First, it is assumed that randomly distributed scatterers give rise to all echoes; thus, the probability that any scatterer is at one position is the same as the probability at any other position. Second, multiple scattering is assumed to be negligible.[11] Third, over the surface of the transducer, the waves scattered by each particle are spherically symmetric; this requires that the scatterer either be monopolar in nature or be sufficiently far from the transducer face that this assumption holds. Finally, the number of scatterers in the volume contributing to the analysis is taken to be Poisson distributed.

The backscatter signal voltage at time t is given by[1]

$$V(t)=\int_{-\infty}^{+\infty} d\omega\, T(\omega)B_0(\omega)e^{-i\omega t}\sum_{i=1}^{M_{\text{all}}}\psi_i(\omega)\times[A(\mathbf{r}_i,\omega)]^2, \tag{1}$$

where $T(\omega)$ is a complex transfer function relating the net instantaneous force on the transducer at the angular frequency ω to the detected voltage. Here, $B_0(\omega)$ is a complex superposition coefficient corresponding to the frequency composition of the emitted pulse. $\psi_i(\omega)$ is the value of the angular distribution factor[11] at a 180° scattering angle for the ith scatterer whose position is $\mathbf{r}_i$. The sum is over all scatterers, M_{all} in space. These scatterers could be identical, or they could consist of a finite number of subsets of scatterers, each subset containing scatterers identical to one another, but unlike those in other sets. The beam pattern of the transducer is accounted for with $A(\mathbf{r},\omega)$, the Rayleigh integral for the case in which the normal component of the velocity at any instant of time is the same at all points on the radiation surface. It is given by

$$A(\mathbf{r},\omega)\equiv\int\int_s ds'\,\frac{e^{ik|\mathbf{r}-\mathbf{r}'|}}{|\mathbf{r}-\mathbf{r}'|}, \tag{2}$$

where the integration is over the transducer surface, $\mathbf{r}'$ points to an element ds' on the transducer surface, and the complex wave number is denoted by $k\equiv\omega/c(\omega)+i\alpha(\omega)$, where $c(\omega)$ is the speed of sound and $\alpha(\omega)$ is the attenuation coefficient.

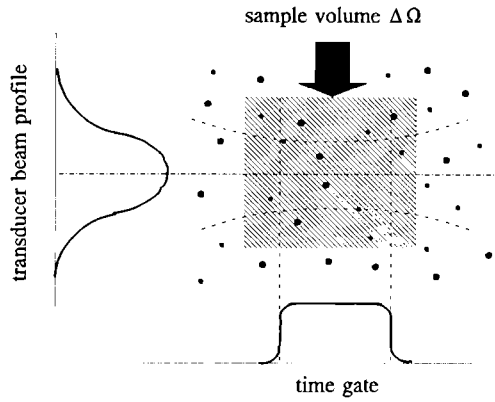

FIG. 1. A volume $\Delta\Omega$ in the medium containing M scatterers. The volume is wide enough compared to the ultrasound beam and extends a sufficient distance axially to include all scatterers contributing to the gated echo signal segment, described in Eq. (3').

Experimentally, the analysis is applied to a segment of the echo signal defined by a time gate. The Fourier transform of the gated echo voltage is given by

$$V_g(\omega)=\int_{-\infty}^{+\infty} d\omega_1\, T(\omega_1)B_0(\omega_1)W(\omega-\omega_1)\times\sum_{i=1}^{M_{\text{all}}}\psi_i(\omega_1)[A(\mathbf{r}_i,\omega_1)]^2, \tag{3}$$

where $W(\omega-\omega_1)$ is the Fourier transform of the gating function. For a rectangular gate, this is simply $W(\omega-\omega_1)=(\tau/2\pi)\text{sinc}[(\omega-\omega')(\tau/2\pi)]$. (The zero of the clock has been set in the middle of the time gate, and the gate duration is τ.)

Let us consider a small volume $\Delta\Omega$ of the medium where there are M scatterers, as shown in Fig. 1. The volume is wide enough compared to the transducer beam and extends a sufficient distance axially to include all scatterers contributing significantly to the time-gated echo signal segment. Thus,

$$V_g(\omega)=\int_{-\infty}^{+\infty} d\omega_1\, T(\omega_1)B_0(\omega_1)W(\omega-\omega_1)\sum_{i=1}^{M}\psi_i(\omega_1)\times[A(\mathbf{r}_i,\omega_1)]^2. \tag{3'}$$

The square of the modulus of the Fourier transform is

$$V_g(\omega)V_g^*(\omega)=\int_{-\infty}^{+\infty} d\omega_1\, T(\omega_1)B_0(\omega_1)W(\omega-\omega_1)\times\int_{-\infty}^{+\infty} d\omega_2\, T^*(\omega_2)B_0^*(\omega_2)\times W^*(\omega-\omega_2)I_2, \tag{4}$$

where I_2 is given by

$$I_2\equiv\sum_{i=1}^{M}\sum_{j=1}^{M}\psi_i(\omega_1)\psi_j^*(\omega_2)[A(\mathbf{r}_i,\omega_1)]^2[A^*(\mathbf{r}_j,\omega_2)]^2.$$

Here, I_2 can be segregated into two parts, one corresponding to incoherent scattering for the subset $i=j$, and the other to coherent scattering for the subset $i\neq j$. Thus,

$$I_2=\sum_{i=1}^{M}\psi_i(\omega_1)\psi_i^*(\omega_2)[A(\mathbf{r}_i,\omega_1)]^2[A^*(\mathbf{r}_i,\omega_2)]^2 + \sum_{i=1}^{M}\sum_{\substack{j=1\\ j\neq i}}^{M}\psi_i(\omega_1)\psi_j^*(\omega_2) \times[A(\mathbf{r}_i,\omega_1)]^2[A^*(\mathbf{r}_j,\omega_2)]^2. \quad (5)$$

In an experiment, a set of gated echo signals is recorded. Each signal corresponds to a distribution of scatterers which is not spatially correlated with that for any other recorded signal in the set. We can write the ensemble average of $V_g(\omega)V_g^*(\omega)$ as

$$\langle V_g(\omega)V_g^*(\omega)\rangle=\int_{-\infty}^{+\infty}d\omega_1\,T(\omega_1)B_0(\omega_1)W(\omega-\omega_1) \times\int_{-\infty}^{+\infty}d\omega_2\,T^*(\omega_2)B_0^*(\omega_2) \times W^*(\omega-\omega_2)\langle I_2\rangle, \quad (6)$$

where

$$\langle I_2\rangle=\left\langle\sum_{i=1}^{M}\psi_i(\omega_1)\psi_i^*(\omega_2)[A(\mathbf{r}_i,\omega_1)]^2[A^*(\mathbf{r}_i,\omega_2)]^2\right\rangle + \left\langle\sum_{i=1}^{M}\sum_{\substack{j=1\\ j\neq i}}^{M}\psi_i(\omega_1)\psi_j^*(\omega_2) \times[A(\mathbf{r}_i,\omega_1)]^2[A^*(\mathbf{r}_j,\omega_2)]^2\right\rangle$$

and $\langle\cdots\rangle$ designates the ensemble average.

Using the fact that M, $\psi_i(\omega)$, and $A(\mathbf{r}_i,\omega)$ are statistically independent random variables, $\langle I_2\rangle$ can be greatly simplified. We have

$$\langle I_2\rangle=\sum_{M=0}^{+\infty}P(M)\left(\sum_{i=1}^{M}\langle\psi_i(\omega_1)\psi_i^*(\omega_2) \times[A(\mathbf{r}_i,\omega_1)]^2[A^*(\mathbf{r}_i,\omega_2)]^2\rangle\right)+\sum_{M=0}^{+\infty}P(M) \times\left(\sum_{i=1}^{M}\sum_{\substack{j=1\\ j\neq i}}^{M}\langle\psi_i(\omega_1)\psi_j^*(\omega_2) \times[A(\mathbf{r}_i,\omega_1)]^2[A^*(\mathbf{r}_j,\omega_2)]^2\rangle\right)$$

$$=\sum_{M=0}^{+\infty}P(M)\left(\sum_{i=1}^{M}\langle\psi_i(\omega_1)\psi_i^*(\omega_2)\rangle_s \times\langle[A(\mathbf{r}_i,\omega_1)]^2[A^*(\mathbf{r}_i,\omega_2)]^2\rangle_r\right)+\sum_{M=0}^{+\infty}P(M) \times\left(\sum_{i=1}^{M}\sum_{\substack{j=1\\ j\neq i}}^{M}\langle\psi_i(\omega_1)\rangle_s\langle\psi_j^*(\omega_2)\rangle_s \times\langle[A(\mathbf{r}_i,\omega_1)]^2\rangle_r\langle[A^*(\mathbf{r}_j,\omega_2)]^2\rangle_r\right), \quad (7)$$

where $P(M)$ is the probability that there are M scatterers in $\Delta\Omega$. Note, the following theorem was employed in the last step: The expectation value of a product of independent random variables equals the product of their expectation values. Here, $\langle\psi_i(\omega)\rangle_s$ is the expectation value of the angular distribution function at 180° for the ith—or any scatterer. This expectation value is related to the scatterer size distribution. Thus, the label i is unnecessary. The function,

$$\langle[A(\mathbf{r}_i,\omega)]^2\rangle_r\equiv\frac{1}{\Delta\Omega}\int\!\!\int\!\!\int_{\Delta\Omega}d\mathbf{r}_i[A(\mathbf{r}_i,\omega)]^2$$

also does not depend on the label i, and we can write $\langle[A(\mathbf{r}_i,\omega)]^2\rangle_r=\langle[A(\mathbf{r},\omega)]^2\rangle_r$. For the same reason the i and j labels can be dropped from all other factors. Then we have

$$\langle I_2\rangle=\sum_{M=0}^{+\infty}P(M)\left(\sum_{i=1}^{M}\langle\psi(\omega_1)\psi^*(\omega_2)\rangle_s\langle[A(\mathbf{r},\omega_1)]^2 \times[A^*(\mathbf{r},\omega_2)]^2\rangle_r\right)+\sum_{M=0}^{+\infty}P(M) \times\left(\sum_{i=1}^{M}\sum_{\substack{j=1\\ j\neq i}}^{M}\langle\psi(\omega_1)\rangle_s\langle\psi^*(\omega_2)\rangle_s \times\langle[A(\mathbf{r},\omega_1)]^2\rangle_r\langle[A^*(\mathbf{r},\omega_2)]^2\rangle_r\right)$$

$$=\left(\sum_{M=0}^{+\infty}P(M)M\right)\langle\psi(\omega_1)\psi^*(\omega_2)\rangle_s\langle[A(\mathbf{r},\omega_1)]^2 \times[A^*(\mathbf{r},\omega_2)]^2\rangle_r+\left(\sum_{M=0}^{+\infty}P(M)M(M-1)\right) \times\langle\psi(\omega_1)\rangle_s\langle\psi(\omega_2)\rangle_s\langle[A(\mathbf{r},\omega_1)]^2\rangle_r \times\langle[A^*(\mathbf{r},\omega_2)]^2\rangle_r. \quad (8)$$

In most experiments the total volume over which data are acquired is much greater than $\Delta\Omega$. Then $P(M)$ is well approximated by the Poisson probability distribution function. Thus,

$$\sum_{M=0}^{+\infty}P(M)M=\langle M\rangle \quad (9)$$

and

$$\sum_{M=0}^{+\infty}P(M)M(M-1)=\langle M\rangle^2. \quad (10)$$

Therefore, we have

$$\langle I_2\rangle=\langle M\rangle\langle\psi(\omega_1)\psi^*(\omega_2)\rangle_s\langle[A(\mathbf{r},\omega_1)]^2[A^*(\mathbf{r},\omega_2)]^2\rangle_r + \langle M\rangle^2\langle\psi(\omega_1)\rangle_s\langle\psi(\omega_2)\rangle_s\langle[A(\mathbf{r},\omega_1)]^2\rangle_r \times\langle[A(\mathbf{r},\omega_2)]^2\rangle_r.$$

The first term involves incoherent scattering, while the second term involves coherent scattering [in our case related to the onset and termination of the time gate (Ref. 1)]. For a sufficiently long gate duration, the coherent term

is negligible compared to the incoherent term.[1] Thus,

$$\langle I_2\rangle \simeq \langle M\rangle \langle \psi(\omega_1)\psi^*(\omega_2)\rangle_s \langle [A(\mathbf{r},\omega_1)]^2 [A^*(\mathbf{r},\omega_2)]^2\rangle_r$$
$$= \Delta\Omega \langle N\rangle \langle \psi(\omega_1)\psi^*(\omega_2)\rangle_s \langle [A(\mathbf{r},\omega_1)]^2 [A^*(\mathbf{r},\omega_2)]^2\rangle_r$$
$$= \langle N\rangle \langle \psi(\omega_1)\psi^*(\omega_2)\rangle_s \times \iiint_{\Delta\Omega} d\mathbf{r} [A(\mathbf{r},\omega_1)]^2 [A^*(\mathbf{r},\omega_2)]^2, \tag{11}$$

where $\langle N\rangle$ is the mean number of scatterers per unit volume.

If the pulse and/or gate durations are long enough compared to the ultrasonic wave period, $W(\omega-\omega')$ and $B_0(\omega)$ will have a very strong peak at the analysis frequency ω, and we can use $\psi(\omega)$ instead of $\psi(\omega_1)$ and $\psi(\omega_2)$ in Eq. (11). We introduce the differential scattering cross section for one scatterer at the frequency ω and a scattering angle of 180°, $\|\psi(\omega)\|^2 \equiv \psi(\omega)\psi^*(\omega)$. The power spectrum of the gated backscattered signal, Eq. (6), can be simplified to

$$\langle V_g(\omega) V_g^*(\omega)\rangle \simeq \langle N\rangle \langle \|\psi(\omega)\|^2\rangle_s \iiint_{\Delta\Omega} d\mathbf{r} \left\| \int_{-\infty}^{+\infty} d\omega_1 \times T(\omega_1) B_0(\omega_1) W(\omega-\omega_1) \times [A(\mathbf{r},\omega_1)]^2 \right\|^2$$
$$= \langle N\rangle \langle \|\psi(\omega)\|^2\rangle_s \iiint_{\Delta\Omega} d\mathbf{r} \|J(\mathbf{r},\omega)\|^2, \tag{12}$$

where $J(\mathbf{r},\omega)$ is given by

$$J(\mathbf{r},\omega) = \int_{-\infty}^{+\infty} d\omega_1 T(\omega_1) B_0(\omega_1) W(\omega-\omega_1) \times [A(\mathbf{r},\omega_1)]^2. \tag{13}$$

B. Computing the effective scatterer number density

In this part, we show that the second and fourth moments of the echo signal can be used to find an effective scatterer number density. The ensemble average of the fourth moment for the set of echo signal segments is given by

$$\langle (V_g(\omega) V_g^*(\omega))^2\rangle = \int_{-\infty}^{+\infty} d\omega_1 T(\omega_1) B_0(\omega_1) W(\omega-\omega_1) \int_{-\infty}^{+\infty} d\omega_2 T^*(\omega_2) B_0^*(\omega_2) W^*(\omega-\omega_2) \times \int_{-\infty}^{+\infty} d\omega_3 T(\omega_3) B_0(\omega_3) W(\omega-\omega_3) \int_{-\infty}^{+\infty} d\omega_4 T^*(\omega_4) B_0^*(\omega_4) W^*(\omega-\omega_4) \langle I_4\rangle, \tag{14}$$

where $\langle I_4\rangle$ is given by

$$\langle I_4\rangle = \left\langle \sum_{i=1}^{M}\sum_{j=1}^{M}\sum_{k=1}^{M}\sum_{l=1}^{M} \psi_i(\omega_1)\psi_j^*(\omega_2)\psi_k(\omega_3)\psi_l^*(\omega_4) [A(\mathbf{r}_i,\omega_1)]^2 [A^*(\mathbf{r}_j,\omega_2)]^2 [A(\mathbf{r}_k,\omega_3)]^2 [A^*(\mathbf{r}_l,\omega_4)]^2 \right\rangle$$
$$= \sum_{M=0}^{+\infty} P(M) \left(\sum_{i=1}^{M}\sum_{j=1}^{M}\sum_{k=1}^{M}\sum_{l=1}^{M} \langle \psi_i(\omega_1)\psi_j^*(\omega_2)\psi_k(\omega_3)\psi_l^*(\omega_4) [A(\mathbf{r}_i,\omega_1)A^*(\mathbf{r}_j,\omega_2)A(\mathbf{r}_k,\omega_3)A^*(\mathbf{r}_l,\omega_4)]^2\rangle \right),$$

and $P(M)$ is the Poisson probability distribution function.

Similar to the derivation of the second moment of the backscatter signal, using the fact that $\psi_i(\omega)$ and $A(\mathbf{r}_i,\omega)$ are independent random variables, and the contributions of terms containing

$$\left\langle \left(\prod_{p=1}^{m} [A(\mathbf{r}_i,\omega_p)]^2 \right) \times \left(\prod_{q=1}^{n} [A^*(\mathbf{r}_i,\omega_{q+m})]^2 \right) \right\rangle$$

are negligible when $m \neq n$ {since the product varies approximately as $\exp[2i(m-n)\mathbf{k}\mathbf{r}_i]$ over the time-gate volume (Ref. 1)}, only three classes of significant (incoherent) terms exist for each M in $\langle I_4\rangle$:[12] (1) M terms for which $i=j=k=l$, denoted by $\langle I_{41}\rangle$; (2) $M(M-1)$ terms for which $i=j\neq k=l$, denoted by $\langle I_{42}\rangle$; and (3) $M(M-1)$ terms for which $i=l\neq j=k$, denoted by $\langle I_{43}\rangle$. Thus, we have

$$\langle I_4\rangle = \sum_{M=0}^{+\infty} P(M) [\langle I_{41}\rangle + \langle I_{42}\rangle + \langle I_{43}\rangle],$$

where $\langle I_{41}\rangle$, $\langle I_{42}\rangle$, and $\langle I_{43}\rangle$ are given by

$$\langle I_{41}\rangle = \sum_{i=1}^{M} \langle \psi_i(\omega_1)\psi_i^*(\omega_2)\psi_i(\omega_3)\psi_i^*(\omega_4)\rangle_s \times \langle [A(\mathbf{r}_i,\omega_1)A^*(\mathbf{r}_i,\omega_2)A(\mathbf{r}_i,\omega_3) \times A^*(\mathbf{r}_i,\omega_4)]^2\rangle_r,$$

$$\langle I_{42}\rangle = \sum_{i=1}^{M}\sum_{\substack{j=1\\ j\neq i}}^{M} \langle \psi_i(\omega_1)\psi_i^*(\omega_2)\psi_j(\omega_3)\psi_j^*(\omega_4)\rangle_s \times \langle [A(\mathbf{r}_i,\omega_1)A^*(\mathbf{r}_i,\omega_2)]^2 \times [A(\mathbf{r}_j,\omega_3)A^*(\mathbf{r}_j,\omega_4)]^2\rangle_r,$$

$$\langle I_{43}\rangle = \sum_{i=1}^{M}\sum_{\substack{k=1\\ k\neq i}}^{M} \langle \psi_i(\omega_1)\psi_i^*(\omega_4)\psi_k^*(\omega_2)\psi_k(\omega_3)\rangle_s \times \langle [A(\mathbf{r}_i,\omega_1)A^*(\mathbf{r}_i,\omega_4)]^2 \times [A^*(\mathbf{r}_k,\omega_2)A(\mathbf{r}_k,\omega_3)]^2\rangle_r.$$

Again use has been made of the theorem that the expectation value of a product of independent random variables equals the product of their expectation values. As in the development of the second moment, the expectation values are independent of the labels i, j, and k; thus we have

$$\langle I_{41}\rangle = M\langle \psi(\omega_1)\psi^*(\omega_2)\psi(\omega_3)\psi^*(\omega_4)\rangle_s \times \langle [A(\mathbf{r},\omega_1)A^*(\mathbf{r},\omega_2)A(\mathbf{r},\omega_3)A^*(\mathbf{r},\omega_4)]^2\rangle_r,$$

$$\langle I_{42}\rangle = M(M-1)\langle \psi(\omega_1)\psi^*(\omega_2)\rangle_s\langle \psi(\omega_3)\psi^*(\omega_4)\rangle_s \times \langle [A(\mathbf{r},\omega_1)A^*(\mathbf{r},\omega_2)]^2\rangle_r\langle [A(\mathbf{r},\omega_3)A^*(\mathbf{r},\omega_4)]^2\rangle_r,$$

and

$$\langle I_{43}\rangle = M(M-1)\langle \psi(\omega_1)\psi^*(\omega_4)\rangle_s\langle \psi^*(\omega_2)\psi(\omega_3)\rangle_s \times \langle [A(\mathbf{r},\omega_1)A^*(\mathbf{r},\omega_4)]^2\rangle_r\langle [A^*(\mathbf{r},\omega_2)A(\mathbf{r},\omega_3)]^2\rangle_r.$$

Inserting the latter relations into $\langle I_4\rangle$ and introducing Eqs. (9) and (10), we have

$$\begin{aligned}\langle I_4\rangle = {} & \langle M\rangle\langle \psi(\omega_1)\psi^*(\omega_2)\psi(\omega_3)\psi^*(\omega_4)\rangle_s\langle [A(\mathbf{r},\omega_1)A^*(\mathbf{r},\omega_2)A(\mathbf{r},\omega_3)A^*(\mathbf{r},\omega_4)]^2\rangle_r \\ & + \langle M\rangle^2\langle \psi(\omega_1)\psi^*(\omega_2)\rangle_s\langle \psi(\omega_3)\psi^*(\omega_4)\rangle_s\langle [A(\mathbf{r},\omega_1)A^*(\mathbf{r},\omega_2)]^2\rangle_r\langle [A(\mathbf{r},\omega_3)A^*(\mathbf{r},\omega_4)]^2\rangle_r \\ & + \langle M\rangle^2\langle \psi(\omega_1)\psi^*(\omega_4)\rangle_s\langle \psi^*(\omega_2)\psi(\omega_3)\rangle_s\langle [A(\mathbf{r},\omega_1)A^*(\mathbf{r},\omega_4)]^2\rangle_r\langle [A^*(\mathbf{r},\omega_2)A(\mathbf{r},\omega_3)]^2\rangle_r.\end{aligned}$$

The two terms containing $\langle M\rangle^2$ contribute equally to $\langle [V_g(\omega)V_g^*(\omega)]^2\rangle$ in Eq. (14), since ω_1 and ω_2 are (exchangeable) dummy integration variables. Introducing this idea, as well as the assumption that both the pulse and gate durations are long compared to the period of the ultrasonic wave, we can use $\psi(\omega)$ instead of $\psi(\omega_1)$, $\psi(\omega_2)$, $\psi(\omega_3)$, and $\psi(\omega_4)$. So the fourth moment of the backscattered signal is given by

$$\begin{aligned}\langle (V_g(\omega)V_g^*(\omega))^2\rangle &= \langle N\rangle\langle \|\psi(\omega)\|^4\rangle_s \iiint_{\Delta\Omega} d\mathbf{r} \left\| \int_{-\infty}^{+\infty} d\omega_1\, T(\omega_1)B_0(\omega_1)W(\omega-\omega_1)[A(\mathbf{r},\omega_1)]^2 \right\|^4 \\ &\quad + 2\left(\langle N\rangle\langle \|\psi(\omega)\|^2\rangle_s \iiint_{\Delta\Omega} d\mathbf{r} \left\| \int_{-\infty}^{+\infty} d\omega_1\, T(\omega_1)B_0(\omega_1)W(\omega-\omega_1)[A(\mathbf{r},\omega_1)]^2 \right\|^2 \right)^2 \\ &= \langle N\rangle\langle \|\psi(\omega)\|^4\rangle_s \iiint_{\Delta\Omega} d\mathbf{r}\|J(\mathbf{r},\omega)\|^4 + 2\langle N\rangle^2\langle \|\psi(\omega)\|^2\rangle_s^2 \left(\iiint_{\Delta\Omega} d\mathbf{r}\|J(\mathbf{r},\omega)\|^2 \right)^2, \end{aligned} \tag{15}$$

where $J(\mathbf{r},\omega)$ is given in Eq. (13).

The ratio of the fourth moment to the square of the second moment is then given by

$$\frac{\langle [V_g(\omega)V_g^*(\omega)]^2\rangle}{\langle V_g(\omega)V_g^*(\omega)\rangle^2} = 2 + \frac{\langle \|\psi(\omega)\|^4\rangle_s}{\langle N\rangle\langle \|\psi(\omega)\|^2\rangle_s^2} \times \frac{\iiint_{\Delta\Omega} d\mathbf{r}\|J(\mathbf{r},\omega)\|^4}{\{\iiint_{\Delta\Omega} d\mathbf{r}\|J(\mathbf{r},\omega)\|^2\}^2}.$$

This equation is similar to that derived by Jakeman[9] to analyze optical scattering from rough surfaces illuminated by single frequency, sinusoidal plane waves. However, here the scattering medium analyzed consists of an extended volume in which scatterers are randomly distributed. Restriction of the received amplitude to that due to scatterers in the volume $\Delta\Omega$ can only be approximated by employing a confined pulsed beam and time gating of the received echoes. The present analysis explicitly accounts for these factors.

If we define the effective scatterer number density $N_{\text{eff}}(\omega)$ as

$$N_{\text{eff}}(\omega) \equiv \langle N\rangle \times \frac{\langle \|\psi(\omega)\|^2\rangle_s^2}{\langle \|\psi(\omega)\|^4\rangle_s} \tag{16}$$

and also define

$$Y(\omega) \equiv \frac{\langle [V_g(\omega)V_g^*(\omega)]^2\rangle}{\langle V_g(\omega)V_g^*(\omega)\rangle^2} - 2, \tag{17}$$

then, we have

$$N_{\text{eff}}(\omega) = Y(\omega)^{-1} \times \frac{\iiint_{\Delta\Omega} d\mathbf{r}\|J(\mathbf{r},\omega)\|^4}{\{\iiint_{\Delta\Omega} d\mathbf{r}\|J(\mathbf{r},\omega)\|^2\}^2}. \tag{18}$$

Equation (18) can be used for determination of the effective scatterer number density, if the pulse and/or gate duration are long enough.

C. Broadband pulses

The method described in Sec. I B may find it greatest use in evaluating the effective scatterer number density when broadband pulses are employed. The results using broadband pulses can yield an effective scatterer number density over a range of frequencies.

For a medium that has a high scatterer number density or for high-resolution imaging, one should use a short duration window instead of a long duration window to reduce the total number of scatterers in each sample volume. In that case, it is necessary to introduce a backscatter frequency-dependent function in Eq. (13) to account for the frequency dependence of scattering. Similar to a previously described method for determining the backscatter coefficient using broadband pulses,[1] the frequency dependence of $\psi(\omega_1)$ can be separated out as a factor $g(\omega_1)$. Thus, we have $\psi(\omega_1) \equiv \psi_0(\omega) g(\omega_1)/g(\omega)$, where ω is the analysis frequency. The quantity $\psi_0(\omega_1)$ will be a more slowly varying function of ω_1 than $\psi(\omega_1)$ if $g(\omega_1)$ is judiciously chosen. This $g(\omega_1)$ can be obtained from determinations of the frequency-dependent backscatter coefficient.

The ratio of the fourth moment to the second moment squared of the backscattered signal is then given by

$$\frac{\langle [V_g(\omega) V_g^*(\omega)]^2 \rangle}{\langle V_g(\omega) V_g^*(\omega) \rangle^2} = 2 + \frac{1}{N_{\text{eff}}(\omega)} \times \frac{\int\int\int_{\Delta\Omega} d\mathbf{r} \|K(\mathbf{r},\omega)\|^4}{\{\int\int\int_{\Delta\Omega} d\mathbf{r} \|K(\mathbf{r},\omega)\|^2\}^2}, \tag{19}$$

where $K(\mathbf{r},\omega)$ is defined as

$$K(\mathbf{r},\omega) = \int_{-\infty}^{+\infty} d\omega_1 \frac{g(\omega_1)}{g(\omega)} T(\omega_1) B_0(\omega_1) W(\omega - \omega_1) \times [A(\mathbf{r},\omega)]^2. \tag{20}$$

Equation (19) would be used to determine the effective scatterer number density using a broadband pulse and a relatively short gate duration window.

II. TESTS OF THE METHOD

A. The experiment

The method for estimating $N_{\text{eff}}(\omega)$ was tested using three phantoms having well-defined scattering properties. The phantoms consist of agar cylinders, 9.0 cm in diameter and 6.0 cm long, with parallel 50-μm-thick Saran windows to allow transmission of ultrasound waves. Embedded in the agar are randomly positioned glass spheres having a diameter distribution that is strongly peaked at 73 μm, as shown in Fig. 2. The mean concentration of scatterers ranges from 140 to 750 scatterers per cm^3.

The differential scattering cross section per scatterer at frequency ω and a scattering angle of 180°, denoted by

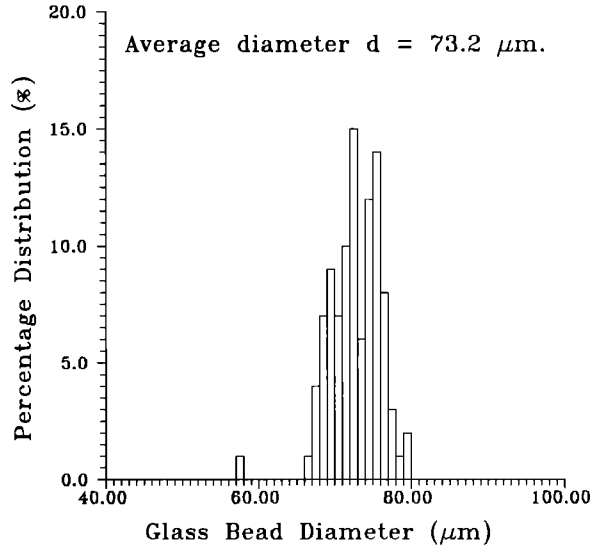

FIG. 2. The size distribution of glass beads in the three phantoms used for testing the data reduction method.

$\|\psi(\omega)\|^2$, was calculated using expressions derived by Faran.[13] The mean and the mean square values of the differential scattering cross section at 180° are given by

$$\langle \|\psi(\omega)\|^2 \rangle = \sum_{i=1}^{L} f_i \|\psi_i(\omega)\|^2,$$

and

$$\langle \|\psi(\omega)\|^4 \rangle = \sum_{i=1}^{L} f_i \|\psi_i(\omega)\|^4,$$

where f_i is the number fraction of scatterers in the ith diameter bin, $\|\psi_i(\omega)\|^2$ is the differential scattering cross section for glass spheres of this diameter and L is the number of bins. Then the theoretical prediction for the effective scatterer number density in each phantom is given by Eq. (16).

The ultrasonic speed and frequency-dependent attenuation coefficients of the phantom materials were measured using a through-transmission technique at 20 °C.[14] The ultrasonic speeds were measured at a single frequency and the attenuation coefficients were measured at 2 and 4 MHz. The attenuation coefficient was assumed to be proportional to the frequency, viz.,

$$\alpha(f) = \alpha_0 f,$$

where α_0 is in dB/(cm MHz), and f is the ultrasound frequency in MHz. Values of ultrasonic properties are given in Table I.

A block diagram of the equipment used is shown in Fig. 3. Two focused transducers were used to transmit pulses and receive the resulting backscattered echo signals. The diameters and radii of curvature of the transducers are given in Table II. The transducers were driven by one-cycle broadband voltage pulses, whose central frequency was the same as the nominal frequency of the transducer. The phantoms were placed near the focal region of the transducers, and echo signal waveforms were recorded with a Lecroy 9400 digital oscilloscope. Waveforms were

TABLE I. Ultrasonic properties of the phantoms used to estimate $N_{\text{eff}}(\omega)$ measurement methods. The attenuation coefficient is described in terms of a constant α_0, corresponding to a linear fitting to experimental values of the form $\alpha(f)=\alpha_0 f$, where f is the frequency in MHz.

Phantoms with different scatterer concentration	Attenuation coefficient α_0 (dB/cm/MHz)	Speed of sound (m/s)	Mass density (g/cm^3)
134 (cm^{-3})	0.068	1554.9±0.5	1.01±0.01
400 (cm^{-3})	0.068	1554.9±0.5	1.01±0.01
750 (cm^{-3})	0.068	1554.9±0.5	1.01±0.01

acquired for 396 different positions, realized by automated translation of the phantoms in a raster fashion over a square matrix, translation being perpendicular to the beam axis of propagation. Each translation step was 3.5 mm. Since the full width at half-maximum (FWHM) of the beam was much less than the translation steps in the interrogated region, successive waveforms were uncorrelated. Also, for each experimental setup $T(\omega)B_0(\omega)$ was determined using a planar reflector as described in Ref. 1.

B. Results

Averages of $V_g(\omega)V_g^*(\omega)$ and $[V_g(\omega)V_g^*(\omega)]^2$ were computed for the data from each phantom; these are denoted by $\langle\langle V_g(\omega)V_g^*(\omega)\rangle\rangle$ and $\langle\langle[V_g(\omega)V_g^*(\omega)]^2\rangle\rangle$. The notation $\langle\langle ... \rangle\rangle$ indicates that these are experimental sample means and are, therefore, approximations of the corresponding means of the parent population denoted by $\langle ... \rangle$ as in Eq. (17). Even for all 396 experimental samples,

$$\Lambda(\omega)\equiv\frac{\langle\langle[V_g(\omega)V_g^*(\omega)]^2\rangle\rangle}{\langle\langle V_g(\omega)V_g^*(\omega)\rangle\rangle^2}-2$$

is a poor approximation of

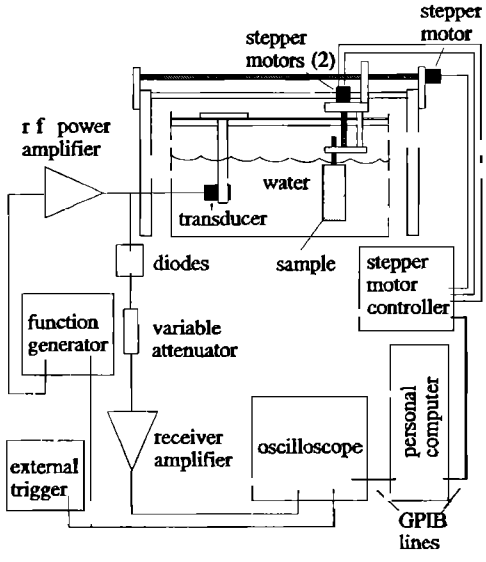

FIG. 3. Diagram of the experimental setup used to collect the echo signals.

TABLE II. Values of the radius of curvature and effective aperture for the transducers used to record echo data from the phantoms.

Nominal resonant frequency (MHz)	Radius of curvature (cm)	Effective aperture (mm)
3.5	9.65±0.07	19.2±0.2
5.0	8.50±0.06	18.6±0.2

$$Y(\omega)\equiv\frac{\langle[V_g(\omega)V_g^*(\omega)]^2\rangle}{\langle V_g(\omega)V_g^*(\omega)\rangle^2}-2.$$

The uncertainty can be reduced either by increasing the number of samples or curve-fitting $\Lambda(\omega)$ over an appropriate range of frequencies around the frequency of interest. We have chosen the latter course. An example is shown in Fig. 4 where third-order polynomial curves have been fit to the $\Lambda(\omega)$ values for two different gate durations. The fitting program used 123 values over the 3-MHz bandwidth. The polynomial curves were then used to determine an experimental value of $N_{\text{eff}}(\omega)$ at the center frequency of the transducer. Standard deviations were determined using the mean square deviation of $\Lambda(\omega)$ from the polynomial fits, averaged over the frequency bandwidth.

Results are summarized in Table III. Columns 2, 3, and 4 are for the 3.5-MHz transducer, while columns 5, 6, and 7 are for the 5.0-MHz transducer. The actual scatterer concentrations of the three phantoms are presented in the second row and the corresponding expected values of $N_{\text{eff}}(\omega)$, obtained from the Faran calculations and acoustical properties of the phantoms, are listed in row 3. Experimental results, along with standard deviations, are presented in rows 4 and 5. They are in reasonable agreement with the expected values of $N_{\text{eff}}(\omega)$ for both transducers. Also, the effective scatterer number density is almost the same at 3.5 and 5.0 MHz, agreeing with the theoretical

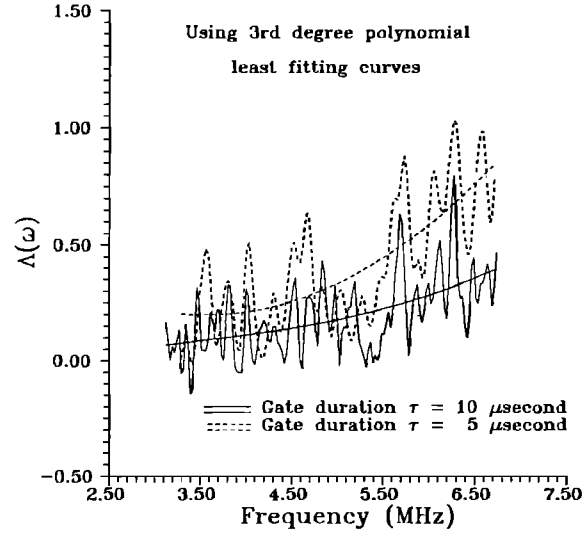

FIG. 4. Typical experimental results of $\Lambda(\omega)$ vs ultrasonic frequency and their polynomial fitting curves. Results for gate durations of 10 and 5 μs are presented. A 5-MHz focused transducer and the 400/cm^3 phantom were used.

TABLE III. Comparisons of the effective scatterer number densities determined from echo data with actual number densities for phantoms containing glass bead scatterers. Comparisons were done both at 3.5 and 5.0 MHz for all three phantoms. $N_{\text{eff}}(\omega)|_{\text{expected}}$ were computed using Eq. (16), while experimental results $N_{\text{eff}}(\omega)|_{\text{experiment}}$ (two lower rows) are presented for 5- and 10-μs time gates. The uncertainties are based on the statistical fluctuations in the experimental results related to their fitting curves.[15]

Ultrasound frequency (MHz)		3.5			5.0	
Scatterer concentration $\langle N \rangle$ (cm^{-3})	134	400	750	134	400	750
$N_{\text{eff}}(\omega)\|_{\text{expected}}$ (cm^{-3})	128	381	714	129	386	724
$N_{\text{eff}}(\omega)\|_{\text{experiment}}$ (cm^{-3}) (gate duration, $\tau=5$ μs)	127 ± 17	420 ± 101	576 ± 256	138 ± 13	356 ± 49	808 ± 166
$N_{\text{eff}}(\omega)\|_{\text{experiment}}$ (cm^{-3}) (gate duration, $\tau=10$ μs)	147 ± 24	414 ± 140	635 ± 491	135 ± 12	371 ± 61	699 ± 201

prediction. The experimental results show that statistical uncertainties are increased when the effective scatterer number density is increased. This is in agreement with predictions by Sleefe and Lele.[7] The inverse of the ratio of the integrals in Eq. (18) may be interpreted as an "effective volume" contributing to the gated signal. The volume ranged from approximately 7 mm^3 for the 5-MHz transducer and 5-μs gate duration to 43 mm^3 for the 3.5-MHz transducer and 10-μs time gate. Thus, the product of the average scatterer number density and effective volume ranged roughly from 1 to 30 in these experiments.

III. SUMMARY AND DISCUSSION

A method of data analysis is described for experimentally determining an effective ultrasound scatterer number density based on the analysis of pulse-echo data. The effective scatterer number density is the actual scatterer number density times a frequency-dependent factor depending on the differential scattering cross section at 180° for each scatterer at the ultrasound frequency involved. If this factor is close to unity, the effective scatterer number density will be close to the actual number density.

The effective scatterer number density is obtained from ratios derived from the second and fourth moments of the backscattered echo signal, when the complex amplitude distribution deviates from Gaussian. Similar approaches have been described previously in the literature, along with experimental verification of the methodology.[4–7,9,12] The major distinctions of the present work are that the derivation retains the frequency dependence of scattering throughout the analysis; scatterers anywhere in the field of the transducer are accounted for without approximations such as using only the -3-dB beamwidth; and the temporal nature of the data acquisition, including representation of a signal selecting time gate applied to the experimental echo signal is accounted for accurately.

The method was tested using phantoms with known actual scatterer concentrations, the spherical glass bead scatterers themselves having a known diameter distribution. The scatterer diameter distribution, along with knowledge of the physical properties of the glass composing the beads, allowed the effective scatterer number densities in the phantoms to be computed directly from first principles. Determinations of the effective scatterer number density using the method of data analysis agreed very well with the independently computed values. Statistical uncertainties, however, increase when the effective number density increases. For a given scatterer number density, uncertainties increase when the effective volume contributing to the time-gated echo signal segments increases.

Further evaluation of this technique will include detailed analysis of the statistical uncertainties, as well as additional tests in phantoms that resemble tissues such as liver more closely. The latter will include phantoms with distributions of different scatterer diameters, likely yielding effective scatterer number densities that depend on the dominant scatterer properties at a particular frequency.

ACKNOWLEDGMENTS

This work was supported in part by NIH Grants R01-CA39224 and R01-CA25634, and by the John R. Cameron Medical Physics Foundation.

[1] E. L. Madsen, M. F. Insana, and J. A. Zagzebski, "Method of data reduction for accurate determination of acoustic backscatter coefficients," J. Acoust. Soc. Am. **70**, 913–923 (1984).

[2] R. Wagner, S. Smith, J. Sandrik, and H. Lopez, "Statistics of speckle in ultrasound B-scans," IEEE Trans. Sonics Ultrason. **SU-30**, 156–163 (1983).

[3] T. A. Tuthill, R. H. Sperry, and K. J. Parker, "Deviation from Rayleigh statistics in ultrasonic speckle," Ultrason. Imaging **10**, 81–89 (1988).

[4] L. Weng, J. M. Reid, P. M. Shankar, and K. Soetanto, "Ultrasound speckle analysis based on the K distribution," J. Acoust. Soc. Am. **89**, 2992–2995 (1991).

[5] R. Kuc, "Ultrasonic tissue characterization using kurtosis," IEEE Trans. Sonics Ultrason. **SU-33**, 273–279 (1986).

[6] G. E. Sleefe and P. P. Lele, "Tissue characterization based on scatterer number density estimation," IEEE Trans. Sonics Ultrason. **SU-35**, 749–757 (1988).

[7] G. E. Sleefe and P. P. Lele, "On estimating the number density of random scatterers from backscattered acoustic signals," Ultrasound Med. Biol. **14**, 709–727 (1988).

[8] L. L. Fellingham and F. G. Sommer, "Ultrasonic characterization of tissue structure in the *vivo* human liver and spleen," IEEE Trans. Sonics Ultrason. **SU-31**, 418–429 (1984).

[9] E. Jakeman, "Speckle statistics with a small number of scatterers," Opt. Eng. **24**, 453–461 (1984).
[10] D. Nicholas, C. R. Hill, and D. K. Nassiri, "Evaluation of backscattering coefficients for excised human tissues: Principle and techniques," Ultrasound Med. Biol. **8**, 7–15 (1982).
[11] P. M. Morse and K. U. Ingard, *Theoretical Acoustics* (McGraw-Hill, New York, 1968), Chap. 8.
[12] E. Jakeman and P. N. Pusey, "A model for non-Rayleigh sea echo," IEEE Trans. Antennas Propag. **AP-24**, 806–814 (1974).
[13] J. J. Faran, "Sound scattering by solid cylinders and spheres," J. Acoust. Soc. Am. **23**, 405–418 (1951).
[14] E. L. Madsen, J. A. Zagzebski, R. Banjavic, and R. Jutila, "Tissue mimicking materials for ultrasound phantoms," Med. Phys. **5**, 390–394 (1978).
[15] J. F. Chen, E. L. Madsen, and J. A. Zagzebski, "Statistical uncertainties in estimates of effective scatterer number density," submitted to J. Acoust. Soc. Am.